Research Square

Preprints are preliminary reports that have not undergone peer review.
They should not be considered conclusive, used to inform clinical practice,
or referenced by the media as validated information.

Fatigue life prediction of ceramic matrix composite materials based on physical constraint multi-scale attention network

Xinyu Feng

XinyuFeng7@163.com

North University of China

Xijing Zhu

North University of China

Yao Liu

North University of China

Chao Yan

North University of China

Research Article

Keywords: Ceramic based composite materials, Fatigue life prediction, Multi scale attention network, Physical constraints, deep learning

Posted Date: March 12th, 2026

DOI: https://doi.org/10.21203/rs.3.rs-9061797/v1

License: This work is licensed under a Creative Commons Attribution 4.0 International License.
Read Full License

Additional Declarations: No competing interests reported.

Fatigue life prediction of ceramic matrix composite materials based on physical constraint multi-scale attention network

Xinyu Feng*,Xijing Zhu,Yao Liu,Chao Yan
School of Mechanical Engineering ,North University of China, Shanxi ,Taiyuan,030051,China
* corresponding author:Xinyu Feng
Xinyu Feng's mail:XinyuFeng7@163.com
Xijing Zhu's mail:XijingZhu9@126.com
Yao Liu's mail:YaoLiu81@163.com
Chao Yan's mail:ChaoYan13@126.com

Abstract: In response to the complexity of fatigue behavior of ceramic matrix composites in high-temperature and high stress environments, the author proposes a fatigue life prediction method based on a physically constrained multi-scale attention network (PC MSANet). The study obtained fatigue data of Cf/SiC materials under multiple working conditions through experiments, and extracted features such as macroscopic stress, time-domain statistics, and frequency-domain energy. The results showed that PC MSANet was significantly better than the comparison model in terms of prediction accuracy and stability, with RMSE and MAE of 477.4 and 338.5, R^2 of 0.975, and CSR satisfaction rate of 99.0%, which was superior to LSTM (RMSE=787.5, R^2 =0.932), MLP (RMSE=849.1, R^2 =0.921), and SVR (RMSE=928.7, R^2=0.906). Further analysis shows that introducing physical constraints can reduce RMSE from 905.6 to 630.0, MAE from 647.7 to 408.3, and R^2 to 0.957. This method achieves high-precision and physically consistent fatigue life prediction, providing a new approach for evaluating the service life of composite materials.

Keywords: Ceramic based composite materials; Fatigue life prediction; Multi scale attention network; Physical constraints; deep learning

1. Introduction

Ceramic based composite materials have become key materials in extreme environments such as aircraft engines and high-temperature structural components due to their excellent high-temperature strength, thermal shock resistance, and corrosion resistance [1]. However, the fatigue behavior of this type of material under cyclic loading exhibits strong nonlinearity,

multiscale, and environmental sensitivity. Its damage evolution involves complex coupling mechanisms such as fiber/matrix debonding, interface slip, and microcrack propagation, making accurate prediction of its fatigue life a major challenge in engineering design and safety assessment [2-3]. Traditional life prediction methods based on physical experiments or phenomenological models often rely on simplified assumptions and specific operating conditions, making it difficult to achieve high-precision and highly generalized life assessment under variable loads and high temperature environments. There is an urgent need to develop new prediction theories that integrate physical mechanisms and data-driven capabilities.

In terms of performance characterization and model construction of ceramic matrix composites, existing research has promoted cognitive progress in this field from different perspectives. Wen et al. revealed the key influence of structural non-uniformity in shaped ceramic matrix composites through a dual-mode non-destructive characterization method, providing experimental evidence for understanding the initial state and performance dispersion of materials [4]. Fang et al. focused on the application of polyborosiloxane in carbon fiber reinforced SiBOC ceramic matrix composites, optimized the material preparation process from the perspective of matrix design and synthesis pathway, and improved the high-temperature stability of the composite material [5]. Miao et al. successfully prepared high entropy ceramic matrix composites through precursor impregnation and cracking process, studied the relationship between their microstructure and properties, and demonstrated the potential application of the new material system in extreme environments [6]. Yan ı komer and Erenturk conducted research on the applicability of ceramic substrates in nuclear waste solidification, expanding the scope of performance evaluation of ceramic materials in multifunctional applications [7]. These studies have made significant progress in material preparation, performance characterization, and mechanism analysis, providing important materials science and experimental foundations for fatigue life prediction.

Although there have been abundant achievements in material preparation and performance evaluation, there are still significant limitations in fatigue life prediction methods for complex working conditions [8]. On the one hand, most existing models still rely on single scale features or simplified damage assumptions, failing to effectively integrate the multi-scale

correlation between macroscopic mechanical responses and microscopic damage evolution; On the other hand, traditional data-driven methods such as support vector regression and multilayer perceptron can capture some nonlinear relationships, but often lack embedding of material physics laws, resulting in biased prediction results that violate physical knowledge in data scarce areas or extreme working conditions [9]. In addition, existing methods have insufficient research on the attention selection mechanism of key features in fatigue processes, making it difficult to adaptively focus on the damage signals that contribute the most to life prediction, which limits the accuracy and robustness of the model. These problems are particularly prominent in complex environments such as high temperature and variable amplitude loading, and have become bottlenecks that urgently need to be overcome in the field of fatigue life prediction of ceramic matrix composites.

In response to the above issues, the author proposes a fatigue life prediction method based on a physically constrained multi-scale attention network, aiming to construct a life prediction framework that combines high accuracy and physical consistency. This method synchronously extracts short-term local features and long-term global evolution laws of material fatigue response through multi-scale convolution structure, and uses multi head attention mechanism to adaptively weight key features and suppress redundant information interference [10]. Furthermore, by introducing physical constraint terms based on Miner's cumulative damage theory, the physical laws of material fatigue failure are embedded into the loss function, so that the model prediction results not only fit experimental data, but also strictly follow the mechanical constitutive relationship. By comparing and verifying with various typical prediction models, the method proposed in this paper has shown significant advantages in prediction accuracy, stability, and physical rationality, providing a new technical path and theoretical support for the reliable evaluation of the service life of ceramic based composite materials in high-temperature and high stress environments.

2. Experimental methods

2.1 Overall Research Framework

The author constructed a fatigue life prediction framework for ceramic matrix composites based on a physically constrained multi-scale attention network (PC MSANet). As shown in

Figure 1, the overall research path includes five steps in sequence: data acquisition and preprocessing, multi-scale feature extraction, attention mechanism modeling, physical constraint embedding, and lifespan prediction and verification [11-12]. Obtain fatigue data of ceramic matrix composite materials through experiments in the early stage, and normalize, denoise, and eliminate outliers to ensure the stability and accuracy of input data; Subsequently, multi-scale convolution structures were used to extract features at different levels, effectively characterizing both macroscopic loading responses and microscopic damage evolution laws [13].

On this basis, a temporal channel joint attention module is introduced to highlight the key features that play a crucial role in fatigue life prediction, while weakening the interference of redundant information. Furthermore, by incorporating the fatigue damage evolution equation and embedding the physical constraint mechanism into the deep learning process, the prediction results not only improve accuracy but also comply with the laws of material mechanics [14]. Ultimately, by integrating multi-scale features, attention mechanisms, and physical constraint models, the prediction and experimental verification of fatigue life of ceramic based composite materials are achieved, providing a reliable basis for the service life evaluation of high-performance composite materials in complex environments.

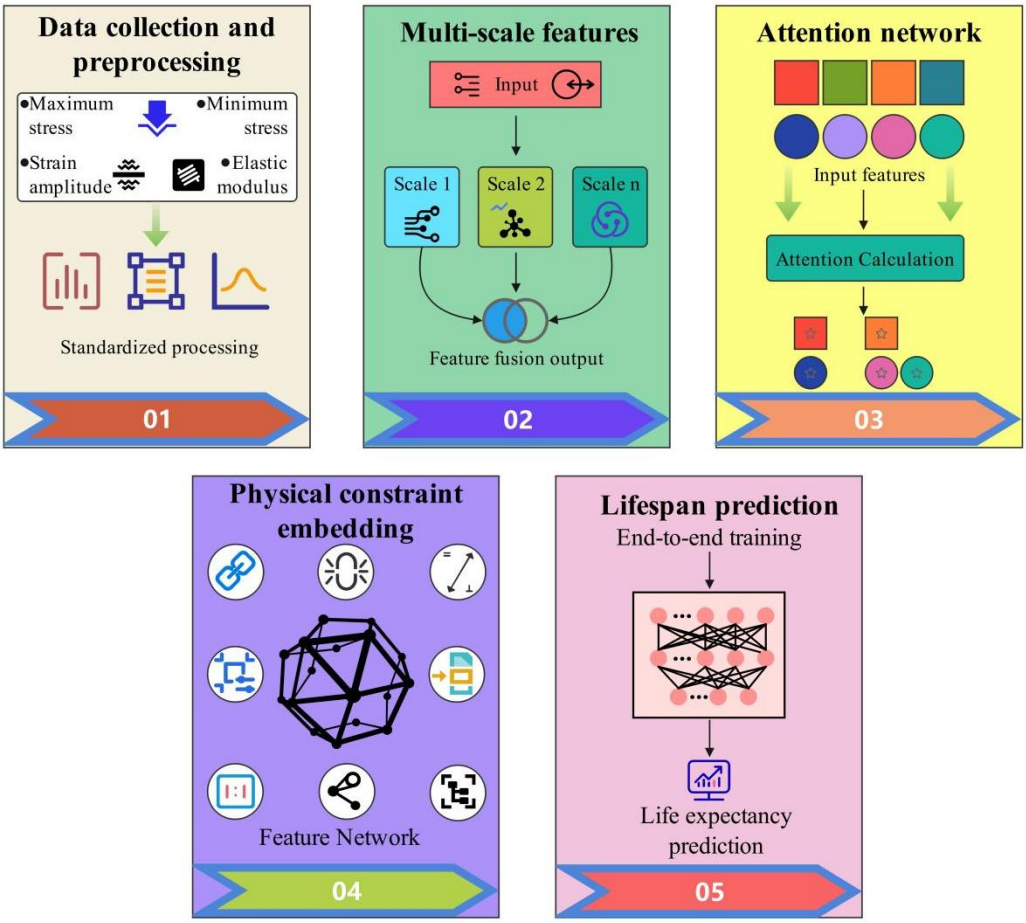


Figure 1 Overall framework diagram of the study (data → multi-scale features → attention network → physical constraints → lifespan prediction)

2.2 Dataset and Experimental Materials

The fatigue behavior of ceramic based composite materials under high temperature, high stress, and complex loading conditions exhibits highly nonlinear and multi-scale characteristics. Therefore, before modeling, it is necessary to ensure that the experimental data has sufficient representativeness and reliability [15]. For this purpose, the author selected typical carbon fiber reinforced ceramic matrix composites (Cf/SiC) and conducted cyclic loading experiments on a high-temperature mechanical testing platform. By controlling the stress amplitude σ_a, loading frequency f, and ambient temperature T, the stress-strain response σ (t), ε (t), and cyclic life N under different operating conditions were obtained. The structure and loading system of the experimental setup are shown in Figure 2, and an example of a typical fatigue loading curve for ceramic matrix composite materials is shown in Figure 3. In the experiment, the fatigue life N_f is defined as the number of cycles corresponding to the

decrease in material stress to α% of the initial peak value σ_0, that is:

$$N_f=\min\{N|\sigma(N)\leq\alpha\sigma_0\},\quad \alpha\in(0,1) \tag{1}$$

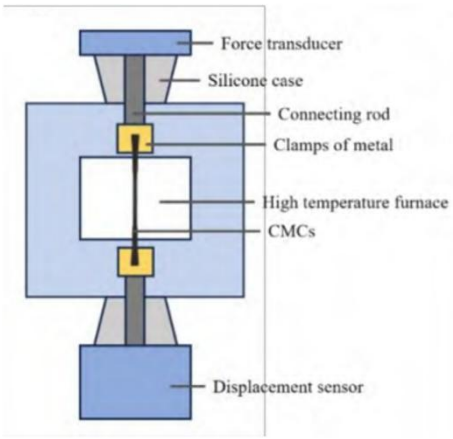


Figure 2 Structure and loading system of experimental setup

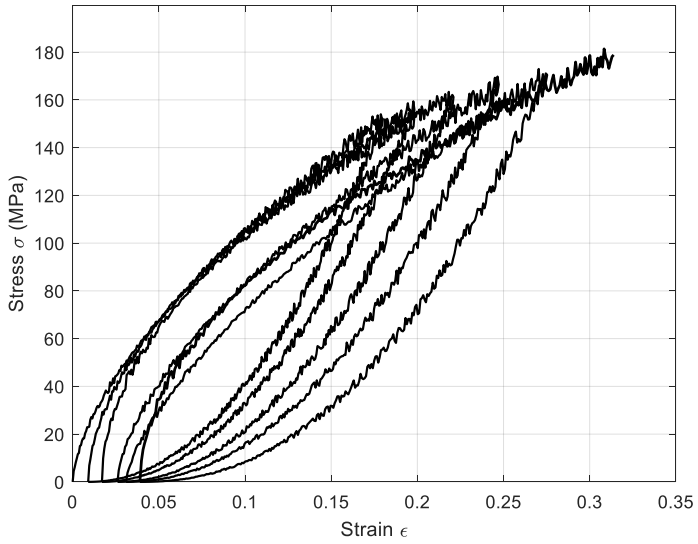


Figure 3 Schematic diagram of cyclic loading unloading stress-strain curve

After obtaining high-quality experimental data, it is necessary to extract effective features to describe the fatigue response of the material. Firstly, in the time domain, the statistical characteristics of the stress signal σ (t) are extracted, including mean μ, standard deviation σ_s, skewness γ_1, and kurtosis γ_2 (see formula 2), which can reflect the overall distribution and abnormal fluctuation characteristics of cyclic loading.

$$\mu=\frac{1}{n}\sum_{i=1}^{n}\sigma_i \tag{2}$$

$$\sigma_s=\sqrt{\frac{1}{n}\sum_{i=1}^{n}(\sigma_i-\mu)^2}$$

$$\gamma_1=\frac{\frac{1}{n}\sum_{i=1}^{n}(\sigma_i-\mu)^3}{\sigma_s^3}$$

$$\gamma_2=\frac{\frac{1}{n}\sum_{i=1}^{n}(\sigma_i-\mu)^4}{\sigma_s^4}-3$$

At the same time, the time-domain signal is converted to the frequency-domain, and the frequency spectrum S (f) is obtained through fast Fourier transform (FFT), and the energy Ek in different frequency ranges is calculated to reveal the frequency characteristics of the micro damage evolution of the material in fatigue cycles, as shown in formula (3).

$$S(f)=\sum_{n=0}^{N-1}\sigma(n)e^{-j2\pi fn/N}$$
$$E_k=\sum_{f\in \mathrm{band}_k}|S(f)|^2 \quad (3)$$

For the convenience of model training and understanding, the author has organized the input features and output labels, as shown in Table 1. The input variables include macroscopic stress characteristics, time-domain statistical characteristics, frequency-domain energy characteristics, and environmental conditions; The output variable is fatigue life Nf.

Table 1 Explanation of Input and Output Variables

Type	Variable name	Description
Macro loading	σ_a	Stress amplitude (MPa)
	f	Loading frequency (Hz)
	T	Temperature (°C)
Time-domain features	μ、σ_s、γ_1、γ_2	Statistical characteristics of stress signals
Frequency domain features	E_1，E_2，...，E_k	Energy in different frequency ranges
Output	N_f	Fatigue life (number of cycles)

After extracting time-domain and frequency-domain features, it is necessary to normalize

and partition the data to ensure the stability and generalization ability of the model training. The original feature matrix X=[x1, x2,..., xn] is normalized using the following formula:

$$\bar{x}_i = \frac{x_i - \min(X)}{\max(X) - \min(X)} \tag{4}$$

Subsequently, outlier detection and removal were carried out, and a stratified sampling strategy was adopted based on stress levels and life intervals to divide the dataset into training, validation, and testing sets in a ratio of 7:2:1. Through the above process, the experimental data covers the fatigue behavior of materials under multiple working conditions, and a high-quality dataset is formed through time-domain and frequency-domain feature extraction, normalization, and hierarchical partitioning, providing a reliable foundation for subsequent multi-scale attention network modeling [16].

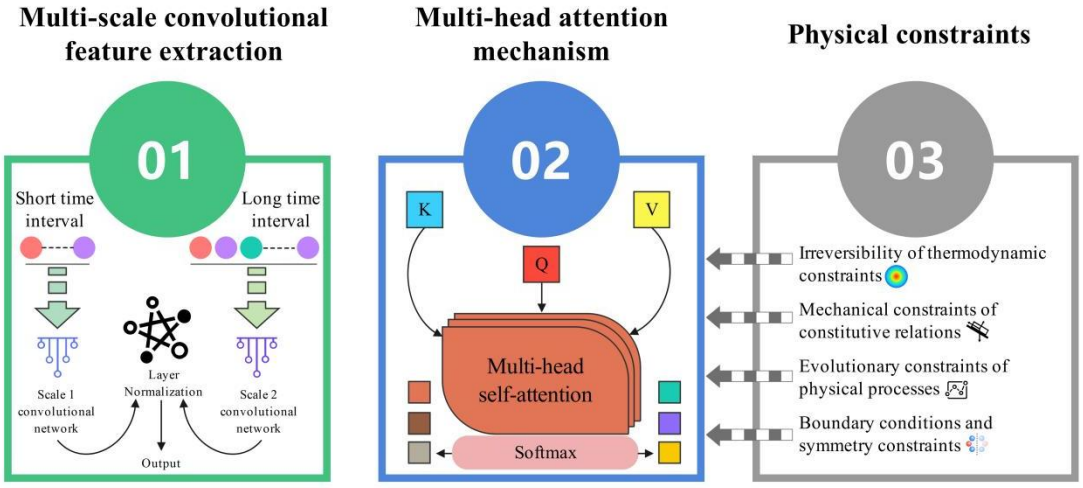


Figure 4 Overall framework of physically constrained multi-scale attention network

Considering that material fatigue signals contain different information at different time scales, the input signal $X \in R^{n \times d}$ is divided into short-term window Xs and long-term window Xl, and local and global features are extracted through convolutional layers, respectively

$$F_s^{(l)} = \sigma\left(W_s^{(l)} * F_s^{(l-1)} + b_s^{(l)}\right)$$
$$F_l^{(l)} = \sigma\left(W_l^{(l)} * F_l^{(l-1)} + b_l^{(l)}\right) \tag{5}$$

Among them, * represents the convolution operation, σ (.) is the activation function, W and

b are the convolution kernel weights and biases, respectively, and l is the convolution layer index. After convolution, the expressive power of multi-scale features is enhanced through residual connections and layer normalization

$$F_s^{(l)}=\text{LayerNorm}\left(F_s^{(l)}+F_s^{(l-1)}\right)$$
$$F_l^{(l)}=\text{LayerNorm}\left(F_l^{(l)}+F_l^{(l-1)}\right) \quad (6)$$

Finally, the short-term and long-term features are merged to form a multi-scale feature matrix F=[Fs, Fl], as shown in Figure 4, which can simultaneously reflect the fatigue evolution characteristics of the material at different time scales.

In order to further highlight the most sensitive feature regions for fatigue life prediction, the model introduces a multi head attention mechanism. For each attention head h:

$$Q_{\text{h}}=FW_{\text{h}}^{Q},\ K_{\text{h}}=FW_{\text{h}}^{K},\ V_{\text{h}}=FW_{\text{h}} \quad (7)$$

$$\text{Attention}_{\text{h}}(F)=\text{softmax}\left(\frac{Q_{\text{h}}K_{\text{h}}^{\text{T}}}{\sqrt{d_k}}\right)V_{\text{h}} \quad (8)$$

After concatenating all the head outputs, the final attention feature is obtained through linear transformation:

$$F_{\text{attn}}=\text{Concat}(\text{Attention}_1,\ldots,\text{Attention}_H)W^{O} \quad (9)$$

Through this mechanism, the model can automatically assign different weights to different features, highlighting the most critical information for life prediction while reducing the interference of redundant features. Visual representation of attention features in Figure 5, seamlessly integrated with multi-scale convolution features.

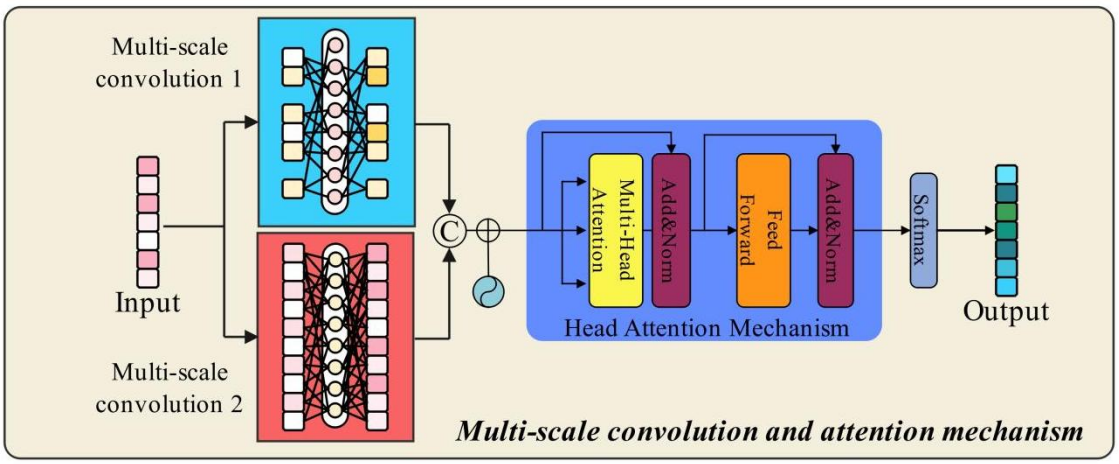


Figure 5 Schematic diagram of multi-scale convolution and attention mechanism

Although data-driven methods can capture complex relationships, relying solely on data may produce predictive results that violate the laws of material mechanics [19]. To this end, the author introduces physical constraints based on Miner's cumulative damage theory in the output layer:

$$D_i=\sum_{j=1}^{m}\frac{n_{ij}}{N_{f,ij}}\leq 1,\quad \widehat{N}_f^{(i)}=\frac{1}{D_i} \tag{10}$$

Among them, n_{ij} is the number of cycles of sample i under stress amplitude σ_j, $N_{f,ij}$ are the experimental lifetimes. This constraint is integrated into the model training through a loss function:

$$\mathscr{L}=\frac{1}{N}\sum_{i=1}^{N}\left(\widehat{N}_f^{(i)}-N_f^{(i)}\right)^2+\lambda\sum_{i=1}^{N}\max(0,D_i-1)^2+\gamma\|\theta\|_2^2 \tag{11}$$

Among them, λ is the physical constraint weight, γ is the L2 regularization coefficient, and θ is the model parameter, ensuring that the model prediction not only conforms to the data trend but also does not violate the physical laws (see Figure 6 for the physical constraint diagram).

The model parameters are updated using Adam optimization algorithm:

$$\begin{aligned} m_t&=\beta_1 m_{t-1}+(1-\beta_1)\nabla_\theta\mathscr{L}_t \\ v_t&=\beta_2 v_{t-1}+(1-\beta_2)(\nabla_\theta\mathscr{L}_t)^2 \\ \widehat{\theta}_{t+1}&=\theta_t-\eta\frac{m_t/(1-\beta_1^t)}{\sqrt{v_t/(1-\beta_2^t)}+\epsilon} \end{aligned} \tag{12}$$

Among them, η is the learning rate, β1,β2, For the first-order and second-order momentum attenuation coefficients, ϵ is the numerically stable term. During the training process, the loss function naturally includes data error terms, physical constraint terms, and regularization terms, achieving accurate modeling of complex nonlinear fatigue behavior [20-21].

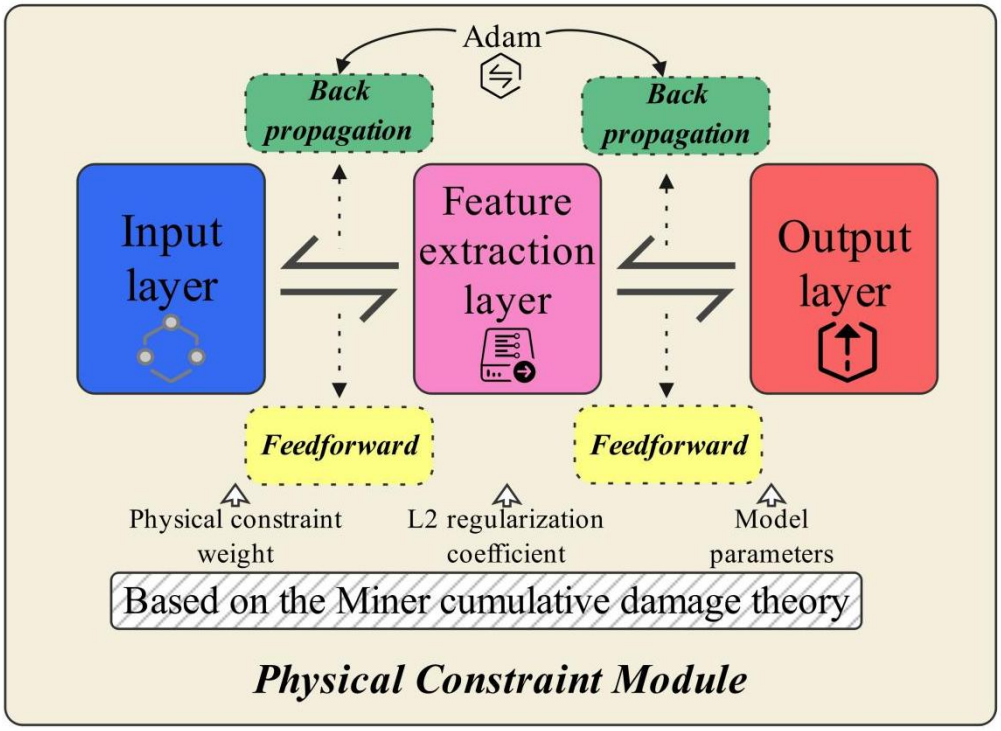


Figure 6 Schematic diagram of physical constraint module

2.4 Comparison Models and Evaluation Indicators

In order to verify the advantages of physically constrained multi-scale attention networks in predicting the fatigue life of ceramic matrix composites, the authors designed three comparative models and quantitatively evaluated the performance of different models using a unified evaluation index [22-23]. Through comparative experiments, the improvement effect of multi-scale feature extraction, attention mechanism, and physical constraints on prediction accuracy can be clearly demonstrated.

The author chooses three typical comparative models:

(1) Support Vector Regression (SVR)

SVR is a traditional nonlinear regression method that can capture the relationship between input features and fatigue life through kernel function mapping

$$\widehat{N}_f=\sum_{i=1}^{N_s}\alpha_i K(x_i,x)+b \tag{13}$$

Among them, x_i is the input feature of the training sample, K (.) is the kernel function, and α_i and b are the model parameters.

(2) Multilayer Perceptron (MLP)

MLP is a typical deep learning method that maps features nonlinearly through multi-layer fully connected networks

$$\widehat{N}_f=\sigma(W_2\cdot\sigma(W_1X+b_1)+b_2) \quad (14)$$

Among them, X is the input feature vector, W1, W2 and b1, b2 are weights and biases, and σ (.) is the activation function.

(3) LSTM model

In order to capture the time series characteristics of fatigue data, an LSTM model is introduced:

$$\begin{gathered} h_t=o_t\odot\tanh(c_t),\quad c_t=f_t\odot c_{t-1}+i_t\odot\tilde{c}_t \\ i_t=\sigma(W_i x_t+U_i h_{t-1}+b_i),\quad f_t=\sigma(W_f x_t+U_f h_{t-1}+b_f),\quad o_t=\sigma(W_o x_t+U_o h_{t-1}+b_o) \end{gathered} \quad (15)$$

In order to ensure the fairness of the comparative experiment, Table 1 summarizes the basic parameter settings of four models (including the physically constrained multi-scale attention network proposed by the author), including input dimension, hidden layer/convolutional layer, number of nodes or convolutional kernels, activation function, learning rate, batch size, and training rounds [24]. By using a unified parameter table, it is possible to visually compare the complexity and training configuration of each model.

Table 2 Basic Parameter Table

Model	Input feature dimension	Hidden layer/Convolutional layer	Node/Convolutional Kernel Count	Activation function	Learning rate	Batch size	Training rounds
Physically constrained multi-scale attention network	d	3 convolutional layers+1 attention layer	64/128/256	ReLU+Softmax	0.001	32	200
LSTM	d	2LSTM layer	128/64	tanh	0.001	32	200
MLP	d	3 fully connected layers	256/128/64	ReLU	0.001	32	200
SVR	d	-	-	-	Kernel function RBF, C=1.0, gamma=scale	-	-

In order to comprehensively measure the performance of the model, the author adopts the following indicators:

RMSE

$$\mathrm{RMSE}=\sqrt{\frac{1}{N}\sum_{i=1}^{N}(\widehat{N}_f^{(i)}-N_f^{(i)})^2} \quad (16)$$

MAE

$$\mathrm{MAE}=\frac{1}{N}\sum_{i=1}^{N}|\widehat{N}_f^{(i)}-N_f^{(i)}| \quad (17)$$

R^2

$$R^2=1-\frac{\sum_{i=1}^{N}(\widehat{N}_f^{(i)}-N_f^{(i)})^2}{\sum_{i=1}^{N}(N_f^{(i)}-\bar{N}_f)^2} \quad (18)$$

Cumulative damage satisfaction rate（CSR）

$$\mathrm{CSR}=\frac{1}{N}\sum_{i=1}^{N}1\,(D_i\leq 1) \quad (19)$$

RMSE and MAE measure the size of prediction error, R2 measures the goodness of fit, and CSR measures whether the model prediction meets physical constraints. These four indicators can comprehensively quantify the performance of different models in terms of accuracy and physical rationality.

3. Experimental results and analysis

3.1 Dataset feature analysis

From the box plot shown in Figure 7, it can be seen that there are significant differences in the distribution interval and dispersion degree of different indicators. Among them, the distribution range of stress amplitude σ_a is the widest (81-179MPa, median 133MPa), reflecting significant fluctuations in loading conditions; The frequency f and temperature T also exhibit a certain degree of discreteness, while other characteristic parameters (such as σ_a, E1-E4) are mainly concentrated in narrow intervals, showing high stability [25]. The violin plot in Figure 8 further reveals the distribution patterns of various variables, with σ a showing a relatively uniform distribution, and the median distribution of f and T tending towards higher values, indicating that the experimental conditions are more concentrated in the higher frequency and high temperature range; The distribution of variables such as E1-E4 is more

concentrated, indicating limited fluctuations under different experimental conditions. Based on the Pearson correlation analysis in Figure 9, it can be found that there is a strong negative correlation between σ_a and the cyclic life N (correlation coefficient close to -1), indicating that stress amplitude is the dominant factor controlling the fatigue life of composite materials; In contrast, the correlation between f, T, μ, σ_s, and other characteristic parameters and N is weak, mostly concentrated in the range of -0.2 to 0.1, showing only slight positive and negative correlations. The correlation between E1-E4 and N is slightly positive, but the degree of action is significantly lower than that of σ_a. From the above, it can be seen that stress amplitude is the key dominant variable affecting the fatigue life of Cf/SiC, while other indicators are more reflected as secondary moderating factors [26-27].

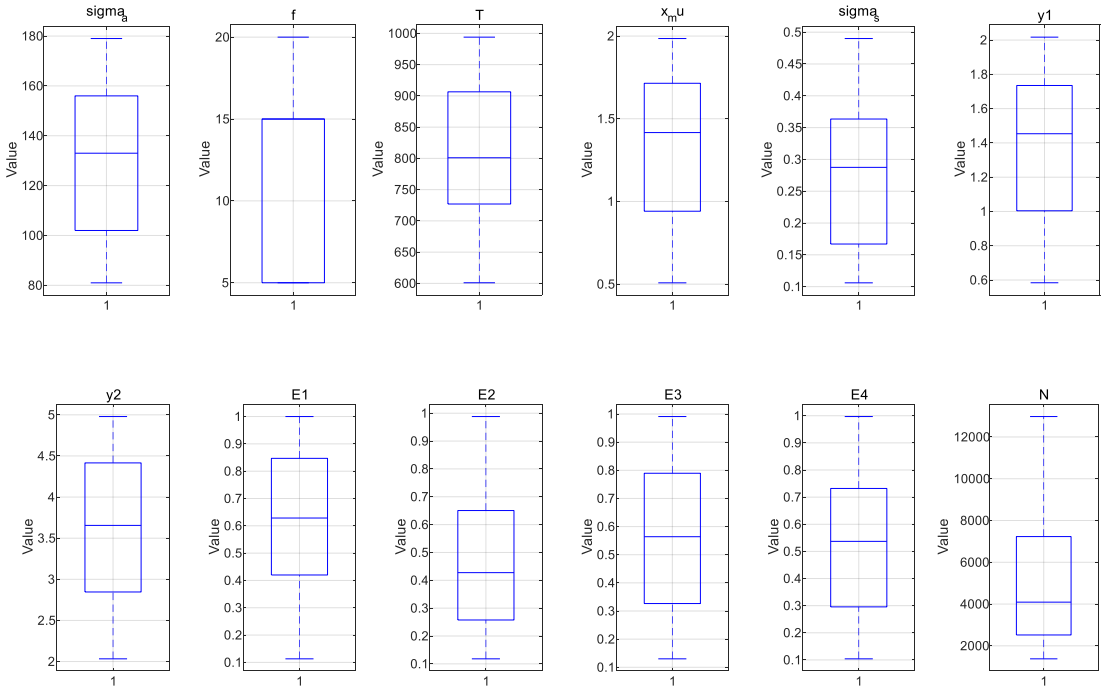


Figure 7 Box plots of different indicators

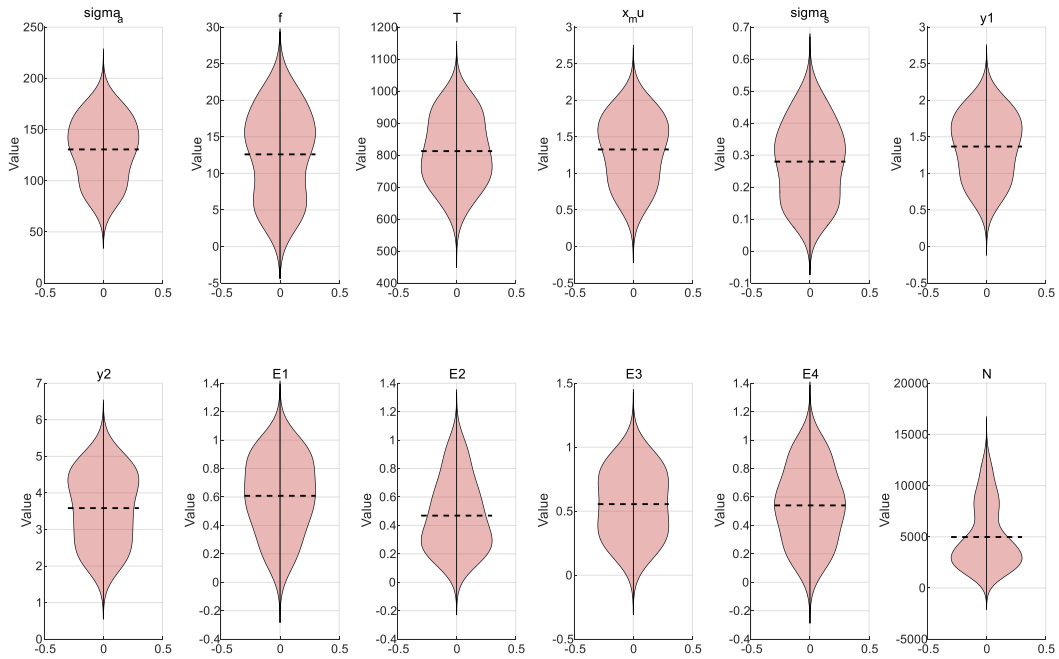


Figure 8 Violin plots with different indicators

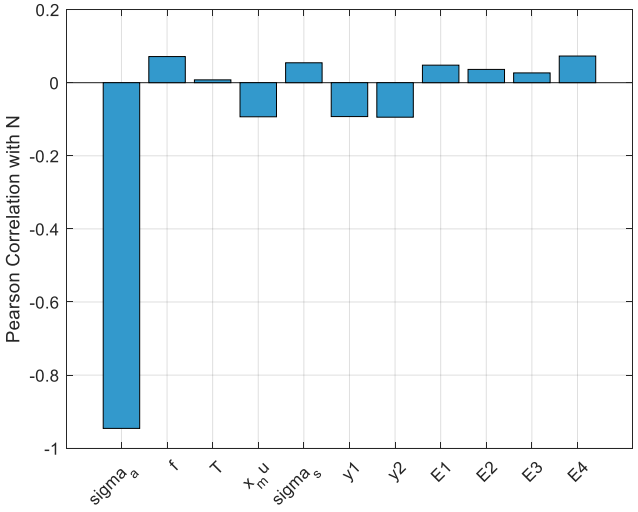


Figure 9 Pearson correlation coefficients between variables and cycle life N

3.2 Comparison of Model Prediction Results

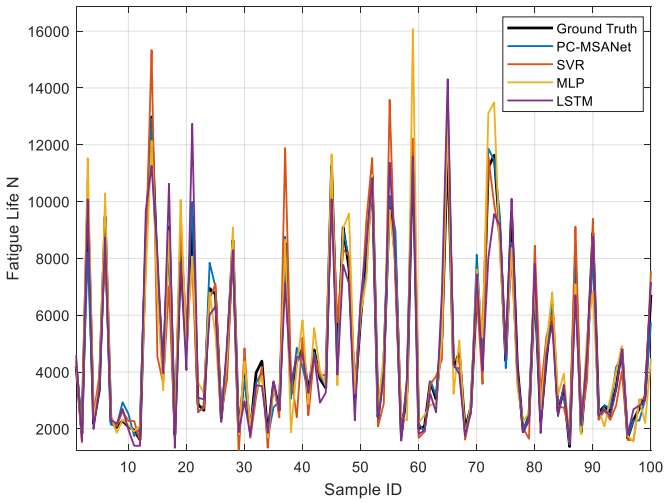


Figure 10 Comparison of real and predicted curves

As shown in Figure 10, the predicted curves of the four models were compared point by point with the true life curves in the sample dimension. It can be seen that the predicted curve of PC MSANet is highly consistent with the real curve as a whole, and can accurately capture the peak and valley positions, demonstrating strong tracking ability; LSTM and MLP can also reflect the overall trend well, but there is a certain deviation in some high lifetime intervals; SVR deviates more significantly in areas with larger local fluctuations. This indicates that PC MSANet outperforms other comparative models in both point by point prediction and overall trend fitting [28-29].

Figure 11 shows the correspondence between the predicted values and the true values of four models. Ideally, all points should be distributed on the reference line of y=x. From the results, the scatter distribution of PC MSANet is the most concentrated, close to the reference line, and has the highest goodness of fit (R^2=0.975); The point distributions of LSTM and MLP are slightly scattered, but overall they still maintain a good correlation (R^2 >0.92); The prediction point deviation of SVR is most obvious, and there is a certain systematic error in the high lifetime region (R^2 =0.906). This result indicates that PC MSANet has significant advantages in overall fitting accuracy [30-31].

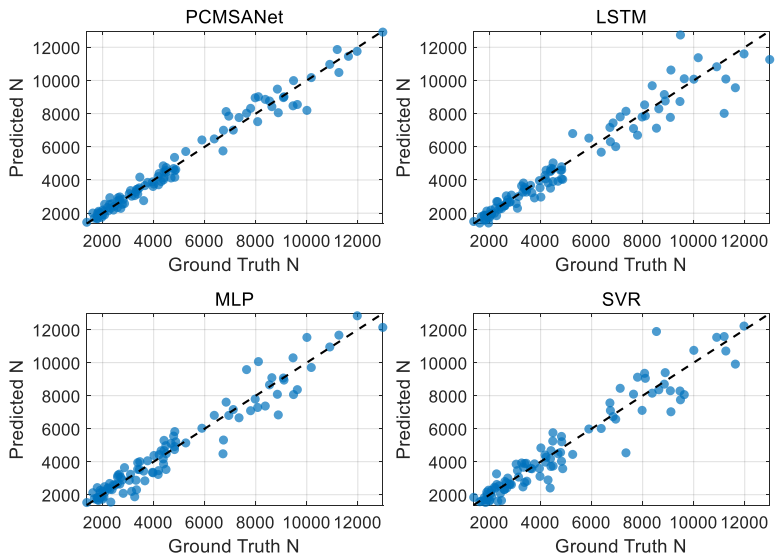


Figure 11 Scatter plot of predicted and true values

Figure 12 compares the distribution characteristics of prediction errors of four models. It can be seen that the error distribution of PC MSANet is the most concentrated, with most errors falling within ± 1000 and the mean close to zero, indicating that the prediction results are stable and reliable; The error distribution range of LSTM and MLP is relatively wider, and there are some points with significant deviations; The error fluctuation of SVR is most obvious, with a longer tail distribution. Combining RMSE and MAE metrics, PC MSANet outperforms other models in error control, further validating its predictive robustness [32-33].

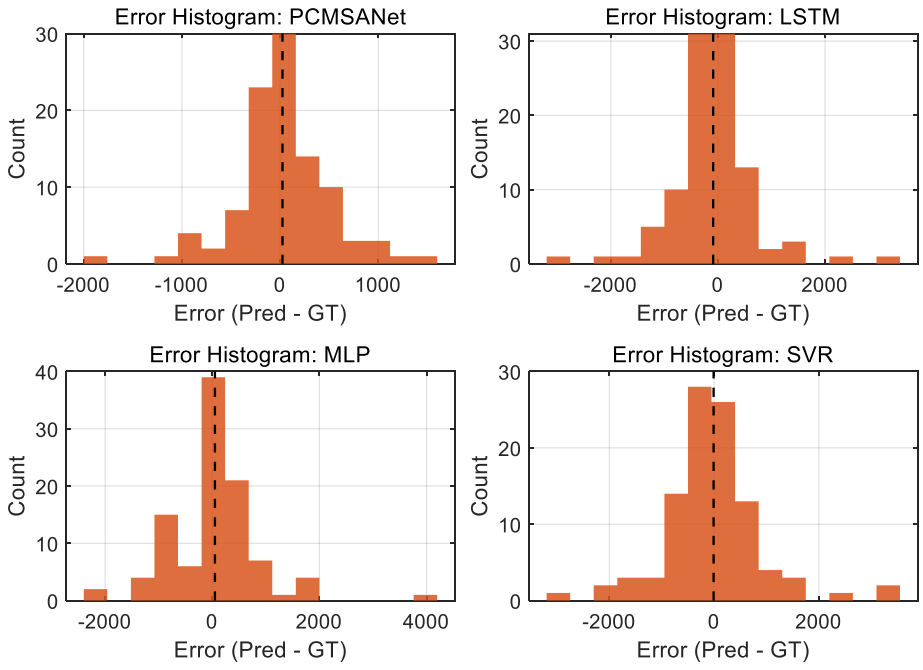


Figure 12 Error distribution of four models in predicting fatigue life

3.3 Analysis of Physical Constraints

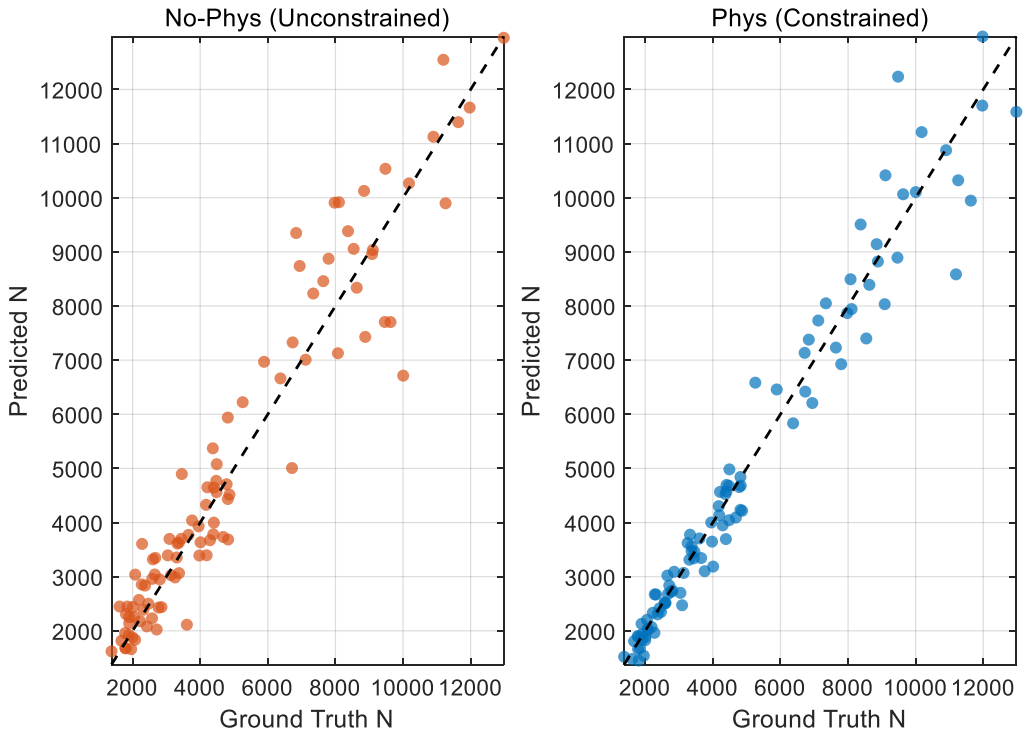


Figure 13 Scatter plot of predicted and true values with and without physical constraints

As shown in Figure 13, without introducing physical constraints (No Phys), the dispersion of predicted points is relatively large, especially in the high lifetime interval where the deviation from the ideal fitting line (y=x) is significant, and the overall goodness of fit is only R^2=0.911; In contrast, after introducing physical constraints (Phys), the predicted points significantly converge near the reference line, with a more concentrated distribution and an improved goodness of fit to R^2 =0.957. At the same time, physical constraints effectively reduced the overall error level, reducing RMSE from 905.6 to 630.0 and MAE from 647.7 to 408.3, while ensuring that all predicted results were within the physically feasible range. This result indicates that physical constraints not only improve prediction accuracy, but also enhance the consistency and reliability of the model [34].

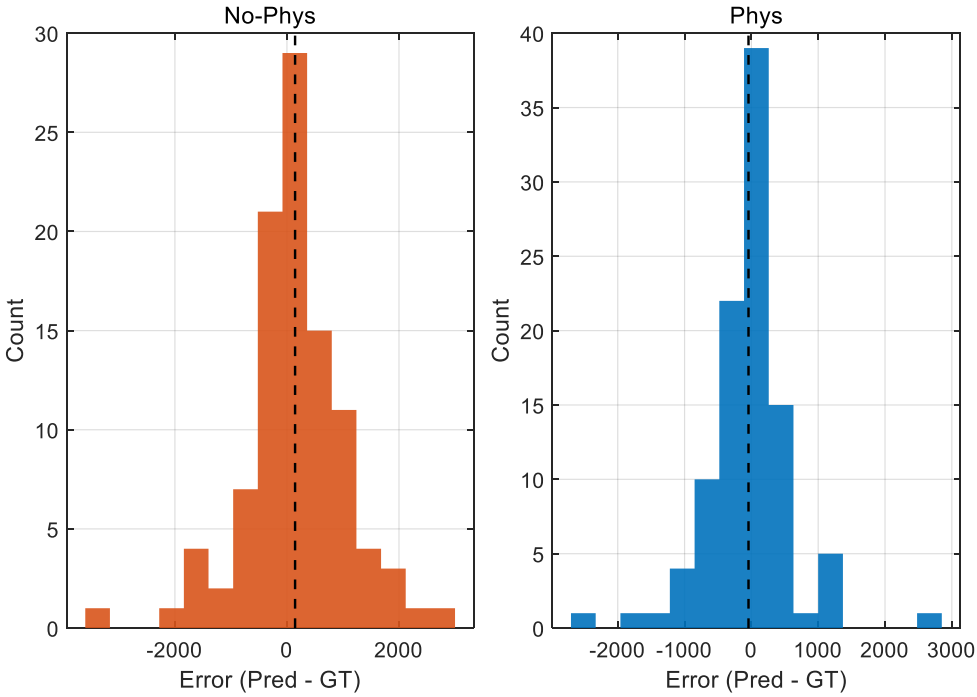


Figure 14 Error distribution of predicting fatigue life with or without physical constraints

Figure 14 shows the error distribution in two scenarios. It can be seen that the prediction error range without physical constraints is wider, the distribution deviates from zero, and the long tail phenomenon is obvious, indicating that the model has significant deviations on some samples. After applying physical constraints, the error distribution significantly narrows, with most errors concentrated within the range of ± 1000 and the mean close to zero, indicating higher prediction stability. This is consistent with the indicators in the table: the introduction of physical constraints not only significantly reduces RMSE and MAE, but also ensures that all predicted values meet the physical rationality under cumulative damage theory (CSR=99%). Therefore, the introduction of physical constraints plays a crucial role in improving the accuracy and physical consistency of prediction results [35].

4. Conclusion

The fatigue life prediction method for ceramic matrix composite materials based on physical constrained multi-scale attention network (PC MSANet) proposed by the author has demonstrated excellent performance in experimental verification. Firstly, from the

comparative experimental results, PC MSANet performs the best in all four evaluation indicators, with RMSE=477.4 and MAE=338.5, significantly lower than LSTM (RMSE=787.5, MAE=509.7), MLP (RMSE=849.1, MAE=575.9), and SVR (RMSE=928.7, MAE=644.7). The goodness of fit R^2 reaches 0.975, far higher than SVR's 0.906, and the CSR satisfaction rate is as high as 99.0%. These results indicate that the model has significant advantages in both prediction accuracy and robustness. Secondly, the introduction of physical constraints further enhances the rationality and stability of the model. Compared with the model without physical constraints, after adding physical constraints, the RMSE decreased from 905.6 to 630.0, the MAE decreased from 647.7 to 408.3, and the R^2 increased from 0.911 to 0.957. At the same time, the CSR satisfaction rate significantly improved, ensuring that the prediction results strictly comply with the Miner's cumulative damage theory. This improvement not only effectively constrains the physical rationality of predictions, but also enhances the model's generalization ability under complex loading conditions. Through comprehensive analysis, it can be concluded that PC MSANet combines multi-scale feature extraction, attention mechanism, and physical constraints, which can achieve both high-precision prediction and physical consistency. It provides a reliable tool for evaluating the service life of ceramic based composite materials in high-temperature and high stress environments. Future research can be further expanded to predict the lifespan of different composite material systems and multi environmental coupling conditions, in order to enhance the generality and engineering applicability of the model.

Fundings: Department of Science and Technology of Shanxi Province, Natural Science Foundation of Shanxi Province (Youth), "Research on Coupled Mechanical Model and Failure Analysis of Aeroengine Ceramic Matrix Composites",Project Approval No:202203021222069;
Department of Science and Technology of Shanxi Province, Natural Science Foundation of Shanxi Province (Youth), "Research on the Integrated Regulation and Synergistic Mechanism of Friction Reduction, Corrosion Resistance, and Wear Resistance on the Surface of 60NiTi Alloy under Complex and Multifactor Marine Environment", Project Approval No:202203021212131".

Conflict of interest: The author declares that they have no competing interest.

Data availability statement: The datasets generated during and/or analysed during the curren t study are available from the corresponding author on reasonable request

Authors' contributions: The author has made important personal contributions to this manuscript.Xinyu Feng: writing and performing surgeries; Xijing Zhu,Yao Liu:data analysis

and performing surgeries;Chao Yan:article review and intellectual concept of the article.

References

[1] Shuoshuo Qu, Yuying Yang, Peng Yao, Luyao Li, Yang Sun & Dongkai Chu. (2025). Fiber reinforced ceramic matrix composites: from the controlled fabrication to precision machining. International Journal of Extreme Manufacturing, 7 (6), 062004-062004. https://doi.org/10.1088/2631-7990/ADEEE1.

[2] Rayva Ranade, Mohamed H Hamza, Luke Borkowski & Aditi Chattopadhyay. (2025). Analysis of damage mechanisms in fiber-reinforced ceramic matrix composites under thermomechanical loading at intermediate and high temperatures. Journal of Composite Materials, 59 (22), 2573-2590. https://doi.org/10.1177/00219983251333104.

[3] Zhijun Wei, Tao Yu & Yumin An. (2025). Research progress on impact resistance properties of fiber-reinforced ceramic matrix composites. Journal of Physics: Conference Series, 3080 (1), 012131-012131. https://doi.org/10.1088/1742-6596/3080/1/012131.

[4] Yintang Wen, Yuhang Du, Wenhan Qu, Jia Gao & Yuyan Zhang. (2025). Dual-Mode Nondestructive Uniformity Characterization of Special-Shaped Ceramic Matrix Composites. Journal of Nondestructive Evaluation, 44 (3), 92-92. https://doi.org/10.1007/S10921-025-01230-9.

[5] Xuan Fang, Jianjun Chen, Zahoor Ahmad, Hao Chen, Jinyu Guo & Hafsa. (2025). Synthesis of polyborosiloxanes for application in carbon fiber-reinforced SiBOC ceramic matrix composites. Materials Today Communications, 47, 113028-113028. https://doi.org/10.1016/J.MTCOMM.2025.113028.

[6] Buragadda V. Rajasekhar, Anurag Kamal, Deepa Devapal & RameshBabu N. (2025). Synthesis of processable matrix resin for carbon fiber-reinforced ultra-high temperature ceramic matrix composites. Journal of the American Ceramic Society, 108 (12), e20697-e20697. https://doi.org/10.1111/JACE.20697.

[7] Huaming Miao, Chenyi Xie, Yanfei Wang, Duan Li & Rongjun Liu. (2025). Fabrication and properties of 3-dimensional 5-directional Cf/(Zr0.2Hf0.2Ta0.2Nb0.2Ti0.2)C-SiC high-entropy ceramic matrix composites by precursor infiltration and pyrolysis process. Ceramics International, 51 (11), 15055-15066.

https://doi.org/10.1016/J.CERAMINT.2025.01.302.

[8] Neslihan Yanikomer & Sema Akyil Erenturk. (2025). Immobilization of simulated cesium wastes in ceramic matrices derived from some natural minerals. Nuclear Engineering and Technology, 57 (5), 103358-103358. https://doi.org/10.1016/J.NET.2024.103358.

[9] Fucai Yang, Xinqiang Cao, Yang Liu & Wenfeng Qiu. (2025). Reaction bonding of oxide/oxide ceramic matrix composites using aluminum nitride as an alumina precursor. International Journal of Applied Ceramic Technology, 22 (4), e15145-e15145. https://doi.org/10.1111/IJAC.15145.

[10] C.T. Brockman, A.S. Almansour, J.D. Kiser, R.K. Goldberg & P. Sarin. (2025). Acoustic emission monitoring of temperature-dependent tensile behavior of unidirectional SiCf/SiC ceramic matrix composites. Journal of the European Ceramic Society, 45 (10), 117350-117350. https://doi.org/10.1016/J.JEURCERAMSOC.2025.117350.

[11] Giacomo Canale, Vitantonio Esperto & Felice Rubino. (2025). A Finite Element Analysis Framework for Assessing the Structural Integrity of Aero-Engine Ceramic Matrix Composite Component Coatings. Metals, 15 (3), 328-328. https://doi.org/10.3390/MET15030328.

[12] Hewei Zhao, Han Zhang, Tong Li, Wenzheng Yin, Mingrui Gao & Shaojia Liu. (2025). Interface Engineering for High Strength and High Toughness Ceramic Matrix Composites.. Chemistry, an Asian journal, 20 (9), e202401805. https://doi.org/10.1002/ASIA.202401805.

[13] Pan Dong, Tianqi Wei, Fei Gao, Yanli Ma, Weiguo Li & Zhaoliang Qu. (2025). Temperature dependent first matrix cracking stress considering fiber fracture for fiber reinforced ceramic composites. Journal of the American Ceramic Society, 108 (7), e20462-e20462. https://doi.org/10.1111/JACE.20462.

[14] Biao Chen, Hang Sun, Yuchen Ye, Chunming Ji, Shidong Pan & Bing Wang. (2025). Research Status and Development Trends of Joining Technologies for Ceramic Matrix Composites. Materials, 18 (4), 871-871. https://doi.org/10.3390/MA18040871.

[15] Xiaopeng Hu, Qing Liu, Liang Chen, Sai Liu, Jinwei Guo & Wang Zhu. (2025). Damage analysis of CVI SiCf/SiCm ceramic matrix composites under thermal shock. International Journal of Fatigue, 194, 108842-108842. https://doi.org/10.1016/J.IJFATIGUE.2025.108842.

[16] Dahui Yu, Yi He & Zhou Li. (2025). Modeling of temperature-dependent first matrix cracking stress in ceramic matrix composites considering fracture surface energy and residual

thermal stress. Ceramics International, 51 (5), 5639-5645. https://doi.org/10.1016/J.CERAMINT.2024.12.011.

[17] Sheng Huang, Le Rong, Zhuoqun Jiang & Yuriy V. Tokovyy. (2024). Inverse Identification of Constituent Elastic Parameters of Ceramic Matrix Composites Based on Macro–Micro Combined Finite Element Model. Aerospace, 11 (11), 936-936. https://doi.org/10.3390/AEROSPACE11110936.

[18] Maojun Li, Yajie Chen, Xiaoyang Jiang & Xujing Yang. (2024). Surface damage characteristics and identification based on acoustic emission in diamond point grinding carbon/carbon ceramic matrix composites. Proceedings of the Institution of Mechanical Engineers, Part B: Journal of Engineering Manufacture, 238 (13), 2014-2025. https://doi.org/10.1177/09544054231209792.

[19] F. Lindner, G. Puchas, F. Wich, S. Hariri & S. Schafföner. (2025). Mechanical and thermal properties as a function of matrix composition of all-oxide ceramic matrix composites fabricated by a sequential infiltration process. Journal of the European Ceramic Society, 45 (3), 116978-116978. https://doi.org/10.1016/J.JEURCERAMSOC.2024.116978.

[20] Jintao Li, Jun Liu, Bo Wang, Yifan Yue, Chengyu Zhang & Tao Suo. (2024). Tensile damage evolution of unidirectional ceramic matrix composites under thermal stress. Ceramics International, 50 (21PC), 43500-43512. https://doi.org/10.1016/J.CERAMINT.2024.08.201.

[21] Thorsten Steinkopff & Roman Keppeler. (2024). Development and validation of damage and failure models for the design of ceramic matrix composite components. International Journal of Applied Ceramic Technology, 22 (1), e14927-e14927. https://doi.org/10.1111/IJAC.14927.

[22] Qi Zhang, Ben Wang, Chang Song, Hao Wang & Zhongao Shi. (2024). Grinding Characteristics and Surface Roughness Modeling of 2.5D Woven SiCf/SiC Ceramic Matrix Composites. International Journal of Precision Engineering and Manufacturing, 26 (2), 1-20. https://doi.org/10.1007/S12541-024-01086-5.

[23] Luis Baier, Martin Frieß, Nils Hensch & Vito Leisner. (2024). Development of ultra-high temperature ceramic matrix composites for hypersonic applications via reactive melt infiltration and mechanical testing under high temperature. CEAS Space Journal, 17 (4), 1-10. https://doi.org/10.1007/S12567-024-00562-Y.

[24] Li Chaofeng, Jiang Yulin, Cheng Hao & Yang Kang. (2024). Free vibration of rotating bifunctional gradient CNTs-reinforced ceramic matrix composites pre-twisted blade in thermal environment. Proceedings of the Institution of Mechanical Engineers, 238 (13), 6355-6376. https://doi.org/10.1177/09544062231222973.

[25] Pietro Galizia, Simone Failla, Cesare Melandri & Diletta Sciti. (2024). Local indentation response of carbon fibers embedded in a harsh environment: The sintered ultra-high temperature ceramic matrix. Journal of the European Ceramic Society, 44 (9), 5347-5357. https://doi.org/10.1016/J.JEURCERAMSOC.2023.12.025.

[26] Jayanta Bhusan Deb, Jihua Gou, Haonan Song & Chiranjit Maiti. (2024). Machine Learning Approaches for Predicting the Ablation Performance of Ceramic Matrix Composites. Journal of Composites Science, 8 (3), 96-. https://doi.org/10.3390/JCS8030096.

[27] Yunguang Zhou , Ji Zou , Chunxue Zhang , Dezhen Li , Lianjie Ma & Ming Li. (2024). Study on grinding removal mechanism and subsurface damage of bionic layered graphene ceramic matrix composites. The International Journal of Advanced Manufacturing Technology, 130 (7), 3837-3849. https://doi.org/10.1007/S00170-023-12897-7.

[28] Yutaro Arai, Manami Saito, Akane Samizo, Ryo Inoue, Keishi Nishio & Yasuo Kogo. (2024). Material design using calculation phase diagram for refractory high-entropy ceramic matrix composites. International Journal of Applied Ceramic Technology, 21 (4), 2702-2711. https://doi.org/10.1111/IJAC.14688.

[29] Xun Sun, Zhenghao Tian, Ru Jiang & Haitao Liu. (2023). Slurry infiltration and sintering cycle-dependent mechanical properties of 3D oxide/oxide ceramic matrix composites. International Journal of Applied Ceramic Technology, 21 (2), 655-663. https://doi.org/10.1111/IJAC.14592.

[30] Qian Hui, Zheng Jincheng, Wang Yusheng & Jiang Dong. (2023). Fatigue Life Prediction Method of Ceramic Matrix Composites Based on Artificial Neural Network. Applied Composite Materials, 30 (4), 1251-1268. https://doi.org/10.1007/S10443-023-10134-8.

[31] Nagaraja Abhilash M. & Gururaja Suhasini. (2023). A progressive damage model for ceramic matrix mini-composites with thick interphases. Journal of the European Ceramic Society, 43 (10), 4336-4348. https://doi.org/10.1016/J.JEURCERAMSOC.2023.03.052.

[32] Rybyanets A. N., Shvetsov I. A., Petrova E. I., Lugovaya M. A. & Shvetsova N. A..

(2023). Ceramic matrix piezocomposites: method of fabrication and microstructure peculiarities. Ferroelectrics, 605 (1), 88-92. https://doi.org/10.1080/00150193.2023.2169014.

[33] Quiney Z., Jeffs S.P., Gale L., Pattison S. & Bache M.R.. (2023). Matrix cracking onset stress and strain as a function of temperature, and characterisation of damage modes in SiCf/SiC ceramic matrix composites via acoustic emission. Journal of the European Ceramic Society, 43 (7), 2958-2967. https://doi.org/10.1016/J.JEURCERAMSOC.2022.10.042.

[34] Newton C.D., Jeffs S.P., Gale L., Pattison S. & Bache M.R.. (2023). Determining the interlaminar tensile strength of a SiCf/SiC ceramic matrix composite through diametrical compression testing. Journal of the European Ceramic Society, 43 (7), 2951-2957. https://doi.org/10.1016/J.JEURCERAMSOC.2022.11.014.

[35] Karadimas George & Salonitis Konstantinos. (2023). Ceramic Matrix Composites for Aero Engine Applications—A Review. Applied Sciences, 13 (5), 3017-3017. https://doi.org/10.3390/APP13053017.